Cryogenics 82 (2017) 83–91

Contents lists available at ScienceDirect

Cryogenics

journal homepage: www.elsevier.com/locate/cryogenics

Research paper

Experimental investigations and validation of two dimensional model for multistream plate fin heat exchangers

Mukesh Goyal [a,b], Anindya Chakravarty [a], M.D. Atrey [b,*]

[a] Cryo-Technology Division, Bhabha Atomic Research Centre, Trombay, Mumbai 400085, India
[b] Mechanical Engineering Department, Indian Institute of Technology Bombay, Mumbai 400076, India

ARTICLE INFO

Article history:
Received 13 June 2016
Received in revised form 1 December 2016
Accepted 31 December 2016
Available online 21 January 2017

Keywords:
Plate fin heat exchanger
Helium liquefier
Helium refrigerator
Experiments

ABSTRACT

Experimental investigations are carried out using a specially developed three-layer plate fin heat exchanger (PFHE), with helium as the working fluid cooled to cryogenic temperatures using liquid nitrogen (LN_2) as a coolant. These results are used for validation of an already proposed and reported numerical model based on finite volume analysis for multistream (MS) plate fin heat exchangers (PFHE) for cryogenic applications (Goyal et al., 2014). The results from the experiments are presented and a reasonable agreement is observed with the already reported numerical model.

1. Introduction

Two-stream (2S) as well as MS compact PFHE having very high effectiveness (>0.95) are generally used in various cryogenic applications such as modern large size helium liquefaction/refrigeration systems. Various secondary parameters such as axial heat conduction (AHC), property variation with temperature and pressure and parasitic heat in-leaks from surroundings, influence the performance of such high effectiveness heat exchangers. A review on heat exchanger thermal hydraulic models for cryogenic applications is presented by Pacio and Dorao [2]. Thermal design methodologies which are available for MS heat exchangers have been reviewed in detail by Das and Ghosh [3]. In order to understand the thermal behavior of a PFHE, it is important to model it correctly taking care of the above mentioned secondary effects. For the design of high effectiveness, numerical models are essential so as to take care of combined effects of various secondary parameters. In order to verify the design, detailed experimental investigations under realistic cryogenic conditions is not available in published literature. Most of the experimental results on PFHE refer either to fin thermo-hydraulic characterization [4–8] or to header configuration and flow pattern studies [9–12]. Recently experimental evaluation of PFHE is reported by Doohan et al. [13]. An experimental study on layer pattern of MSPFHE to test the optimality of the stacking pattern designed using genetic algorithm is conducted by Wang et al. [14].

A numerical model for MSPFHE, which explicitly accounts for secondary parameters like AHC through heat exchanger metal matrix, parasitic heat in-leak from surroundings, and variable fluid properties/metal matrix conductivity, was earlier proposed and reported by the authors [1]. In this model, the heat exchanger core is discretised in both the axial and transverse directions. The use of fin efficiency term is eliminated because the fins are discretised in the transverse direction due to which the effects of transverse heat conduction/stacking pattern is taken care of. Based on the same reported model, a numerical tool was developed for rating calculations of PFHE with special reference to helium cryogenic systems. The numerical model was validated against results obtained using commercially available software Aspen MUSE™ [15]. The model was further applied to study lateral thermal profiles in MSPFHE using sample heat exchangers. However, the numerical model needed to be backed up with detailed experimentation at cryogenic temperatures. In order to validate the model, a full-fledged closed loop low temperature experimental test facility is developed in our laboratory. The work presented in this article details the experimental work and the comparison of experimental results with the predictions obtained from the mentioned numerical model.

* Corresponding author.
E-mail address: matrey@me.iitb.ac.in (M.D. Atrey).

http://dx.doi.org/10.1016/j.cryogenics.2016.12.005
0011-2275/

2. Numerical model and solution method [1]

Alternate layers of corrugated die-formed metal sheets (the fins) separated by flat metal separation sheets (the plates) are stacked together in a PFHE. Fig. 1 describes a simplified cross-sectional model of a sample PFHE with three layers. For the development of numerical model, it was assumed that every fin in a layer at a particular cross-section exhibits a similar thermal behavior and temperature profile. Therefore, it is possible to represent the fins in a particular layer through one equivalent fin with a thickness equal to the total fin thickness and the heat transfer area equal to the total heat transfer area of all the fins. The heat exchanger is discretised in both axial as well as lateral directions.

In each of the volume elements of the metal matrix, there exists 2D heat conduction (along the length of heat exchanger as well as along the lateral direction as represented by X and Y axes respectively in Fig. 1).

Discretised energy balance equations for each volume element are derived in finite difference form. Due to the 2D discretisation of the domain, it is possible to explicitly incorporate AHC, variable fluid/metal properties, parasitic heat in-leak from surroundings and transverse heat conduction. In the reported model, the system of discretised energy balance equations is solved iteratively using reasonable initial guesses with suitable relaxation factors for metal and fluid nodes. In the developed code, the numerical technique is implemented through visual basic. The computer program uses MSEXCEL® for user interaction. Thermo-physical properties of the fluids are evaluated using GASPAK® [16]/HEPAK® [17]. The thermal conductivity of aluminium (Al) (construction material of the developed PFHE) is evaluated using the empirical correlation from NIST [18]. Offset strip fins are used in the developed PFHE. For heat transfer and flow friction characteristics, well known Manglik and Bergles correlations are used [19]. The model predicts the temperatures of different streams and the end plate temperatures along the length of the PFHE for the given flow rates and inlet temperatures of different fluid streams.

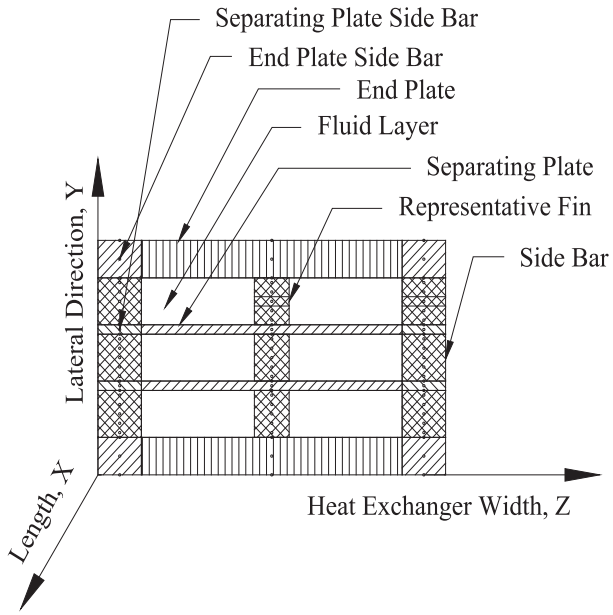

Fig. 1. Simplified cross-sectional model of a sample PFHE with three layers [1].

3. Design and fabrication of major components

3.1. Plate fin heat exchanger

A three-layer vacuum brazed aluminium PFHE is specially developed for model validation experiments. Table 1 provides the details of the heat exchanger core of the developed PFHE. The PFHE core including fins is made of Al-3003, separating plates are made of Al-3003 coated with Al-4104, headers, pipes and other pressure containing parts are made of Al-5052. Pneumatic testing of the PFHE is carried out as per the ASME Boiler and Pressure Vessel Code Section VIII, Div. I [20]. Leak testing is done by soap bubble test and helium mass spectrometric leak detector (MSLD), where leak tightness of the PFHE is found to be better than 10^{-6} mbar l/sec for inter-stream leakages and external leakages. Above mentioned tests are performed at 15 bar (g) pressure. For leak detection using MSLD, detector probe method is used followed by sniffer probe method. In the detector probe method, individual layers are sequentially evacuated and connected with MSLD while the helium gas is spread over the outer joints as well as in the layers not being evaluated. External hood is also used to measure the global leak rate from the atmosphere. In the sniffer probe method, central layer is pressurised with 15 bar (g) of helium gas and helium is sniffed in the other two layers. Global external leak is also evaluated using sniffer probe (hood method) of MSLD, in this case all the layers are pressurised with 15 bar (g) of helium gas. Developed three-layer PFHE is shown in Fig. 2.

3.2. Test cold box

A cold box is designed and fabricated for the experimental test facility. The fabricated cold box is a cylindrical vessel with 800 mm OD, 4 mm thickness and 1700 mm height. It has 25 mm thick flat bottom head, 25 mm thick top ring flange with 800 mm ID and 900 mm OD, top flat head with 25 mm thickness, 900 mm OD and appropriate holes for various openings. Lugs support suitable for fork lift, are provided in the design. The cold box is designed for both internal and external pressures. Under normal working conditions, the cold box is under vacuum, therefore, it is designed for 1 bar external pressure. To avoid damage due to accidental pressurization, it is designed for 1 bar internal pressure. Mechanical design and pneumatic testing are done as per ASME Boiler and Pressure Vessel Code Section VIII, Div. I [20]. A turbo molecular pump (TMP) backed up by a rotary vane pump (RVP) is used for evacuating the cold box. Charcoal packets in contact with LN_2 bath are kept in the vacuum space for long term vacuum retention. A Pirani gauge and a Penning gauge are used for vacuum measurement of the cold box. 1″ safety plate is used for accidental pressurization of cold box. This safety plate remains open under positive

Table 1
Details of the heat exchanger core of the developed PFHE.

Description	Value
Heat Exchanger Matrix Metal	Aluminium (3003)
Core Length	1200 mm
Core Width	184 mm
Side Bar Width	8 mm
Total Width	200 mm
Separating Plate Thickness	0.8 mm
End Plate Thickness	3.8 mm
Fin Type	Offset strip fins
Fin Metal Thickness	0.2 mm
Fin Height	6.3 mm
Serration Length	3 mm
Fin Pitch	1.4 mm

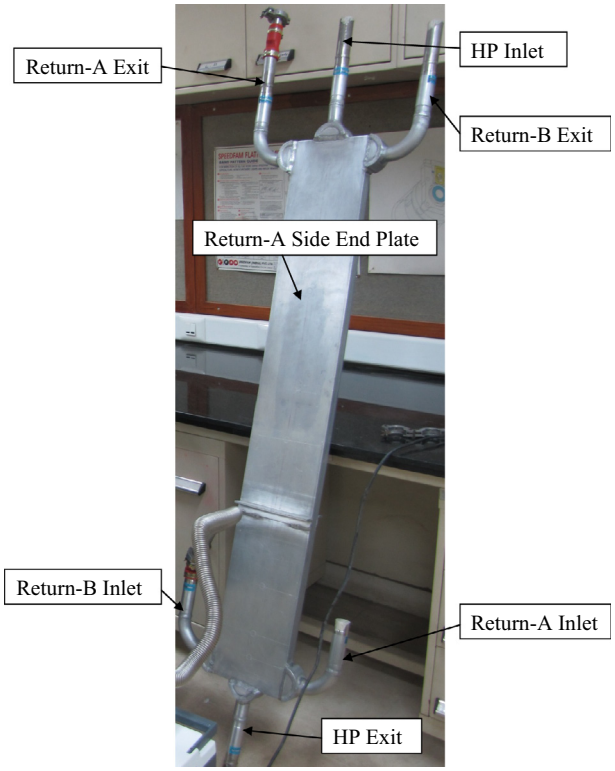

Fig. 2. Developed three-layer PFHE.

pressure inside the cold box and becomes leak-tight when there is vacuum inside the cold box.

A LN_2 bath with approx capacity of 40 L (∅273 mm OD, 800 mm cylindrical height, 2 mm thick shell with 2 mm thick tori-spherical heads) is used for cooling the helium stream. To attain near LN_2 temperatures, the helium stream flows through a helical coiled tube which is housed in the LN_2 bath. The helical coiled tube is made from 1/2″ schedule-10, SS-304L pipe (∅200 mm PCD X 8 turns). A charcoal adsorber (CA) is used in the test facility to remove impurities in the helium gas.

4. Experimental test facility

4.1. Process schematic

The process schematic of the test facility used for conducting experimental trials is shown in Fig. 3. The test facility uses helium as process gas. LN_2 is used for cooling of incoming helium stream. Experiments are conducted at LN_2 temperatures with a three-layer PFHE. A three-stream He/He/He PFHE is shown in the process schematic.

The process fluid (helium) is circulated in a closed loop using an oil flooded helium screw compressor having a fine oil removal system to reduce the oil impurities to ppb level. Compressed high pressure (HP) helium enters the PFHE which is housed in the cryogenic cold box. This HP gas constitutes the HP stream of the three-layer PFHE. The cryogenic cold box is a super insulated vacuum vessel, which, along with the PFHE, also houses a LN_2 bath and a CA at near LN_2 temperature. High pressure exit helium gas from the PFHE enters a helical coiled tube kept in a cylindrical LN_2 bath.

Inside the helical coiled tube, the high pressure helium gas attains near LN_2 temperature. HP helium gas exiting from the helical coiled tube enters the activated CA, where impurities in the helium gas are adsorbed. This HP helium stream, at the exit of CA, is bifurcated using control valves BSCV-01 and BSCV-02. Apart from bifurcating the HP stream, BSCV-01 and BSCV-02 are also used for pressure reduction to obtain the LP streams. These bifurcated streams form the counterflow LP return streams of the PFHE under investigation.

Control valves are used to create different test cases for experiments such as two-stream balanced flow and imbalanced flow cases and three-stream balanced flow case. For the balanced flow two-stream case, control valves BSCV-01 and BSCV-02 remain fully opened and control valve CV-101 remains fully closed. In this case, the mass flow rates and other process parameters for both the LP return streams are same and the total mass flow rates of the LP streams is equal to that of the HP stream. For imbalanced flow experiments, control valve CV-101 is utilized. Using this valve, additional flow can be directed to the LP streams from the intermediate pressure buffer vessel of the compressor control system or a part of the flow from the exit of CA can be directed to the room temperature LP header. For three-stream case, heat capacity rate ratio between the two low pressure return streams is controlled with the help of control valves BSCV-01 and BSCV-02. Flow measurement system is provided for all the three streams and also that of the evaporated LN_2.

Effectiveness of the heat exchanger is evaluated using terminal temperature measurements with Platinum Resistance Sensors (PT-100). Temperature profile along the length of the heat exchanger is found with the help of a series of PT-100 sensors mounted on the both end plates of the heat exchanger. Apart from the exit temperatures of various streams, temperature profiles along the length of the end plates of the PFHE are used for validation of the numerical model.

4.2. Instrumentation and accessories

Orifice meters are used to measure the flow rates of HP, both return LP streams and N_2 vapour. Fuzi make differential pressure transmitters (accuracy: 0.065% of FS) are used to measure the pressure drops across the orifice meters. Orifice meter for the HP flow measurement is calibrated by Fluid control research institute (FCRI), Palakkad (India). Expanded uncertainty for the orifice meter is 0.26% of reading (coverage factor, k = 2). All other orifice meters are calibrated against this orifice meter.

Absolute pressure transmitters (ABB make, accuracy: 0.1% of FS) are used to measure the inlet pressure of HP stream and the exit pressures of return LP streams. Fuzi make differential pressure transmitters (accuracy: 0.065% of FS) are used to measure the pressure drops across return A and return B streams. ABB make differential pressure transmitters (accuracy: 0.1% of FS) is used to measure the pressure drop across HP stream.

PT-100 temperature sensors (Make: Heraeus sensor technology, C-220 series, thin-film, Class B PRTDs) are used for temperature measurements at the inlet and exit of the PFHE as well as along the length of the PFHE. Accuracy of the mounted temperature sensors is ±[0.3 + 0.005|t|] °C. Multipin ceramic feed-throughs are used to take out temperature sensor leads from the cold-box to outside.

Alcatel make MSLD is used for leak testing of the PFHE, cold box and piping. Linde make multicomponent impurity detector and Shaw make moisture meter are used to measure the impurities in the helium streams. Long stem bellow sealed valves (BSCV-01 and BSCV-01) are used for flow and pressure control.

4.3. Mounting and assembly of test PFHE in the cold box

The three-layer PFHE is mounted in the cold box where closed loop low temperature experiments can be carried out. The inner layer of the three layers forms the HP stream of the heat exchanger while the outer two layers constitute the two LP return streams.

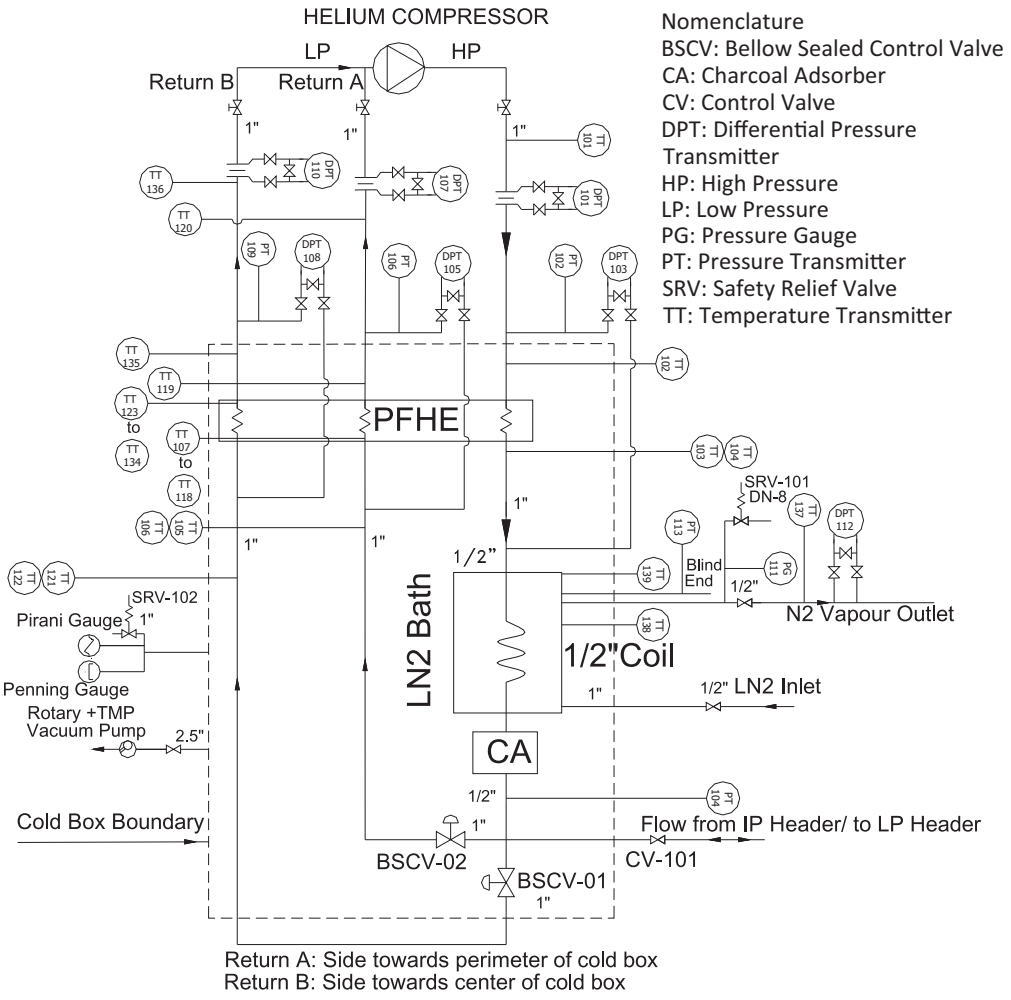

Fig. 3. Process schematic of the test facility.

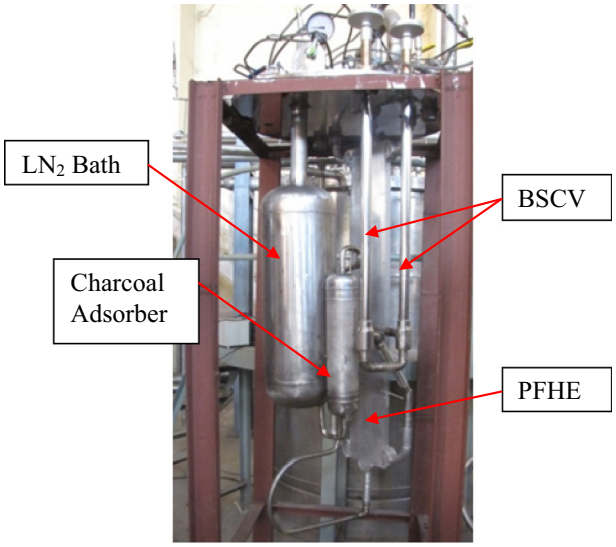

Fig. 4. The cold box piping with three-layer PFHE under investigation.

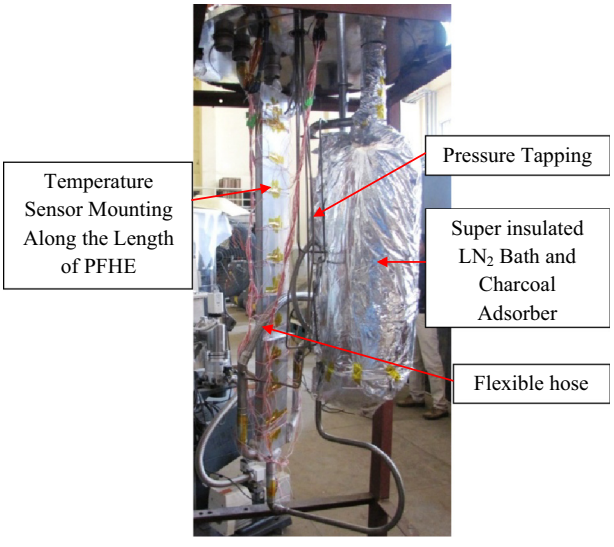

Fig. 5. The cold box piping with super insulated LN_2 bath and temperature sensors mounted in the PFHE.

Fig. 4 shows the cold box piping in which the PFHE with three layers is mounted. The LP side towards the periphery of the cold box is designated as return-A stream and that towards the centre of the cold box is marked as return-B stream. Fig. 5 depicts the cold box piping in which the CA and the LN_2 bath are seen wrapped with multilayer super-insulation. PT-100 sensors are also mounted on the three-layer PFHE. The completed piping assembly wrapped

with super insulation is shown in Fig. 6. The entire facility, completed and ready for experiments, with the cold box, evacuation system, LN_2 filling system, data logging and instrumentation system, etc. is shown in Fig. 7.

5. Experimental results and discussions

Experiments at LN_2 temperatures are carried out with the three-layer PFHE described earlier. Experimental results are compared with the predictions obtained using the reported model [1]. The comparison is carried out with respect to exit temperatures of various fluid streams as well as end plate temperature profiles along the length of the PFHE. In the experimental test facility, the PFHE is housed in a super insulated cold box. Vacuum in the cold box is maintained in the 10^{-6} mbar ranges and 40 layers of aluminised Mylar super-insulation is used in the PFHE. Heat in-leak in the PFHE will be less than 1 W/m^2. Therefore, heat in-leak is neglected for the predictions and comparisons. However, heat in-leak can be an input to the developed 2-D numerical model [1].

5.1. Balanced flow two-stream case

Initially, both BSCV-01 and BSCV-02 are kept fully opened and mass flow rate is slowly increased from 0 g/s to 13 g/s. At each step, steady state is achieved before further increasing the mass flow rate. Table 2 presents the steady state process data at various mass flow rates. For both the LP return streams, the mass flow rates and other process parameters are deliberately kept the same so that a standard two-stream heat exchanger effectiveness (actual heat transfer/maximum possible heat transfer) definition can be applied. A comparison between the exit temperatures obtained experimentally with those computed, using the 2-D numerical model [1] as well as the commercial software Aspen MUSE™ [15], for the same inlet conditions, are presented in Table 2.

Heat exchanger effectiveness values computed using the measured process data during the course of the experiments described in this article are compared to effectiveness values computed using the 2-D numerical model [1] as well as Aspen MUSE™ [15]. The results are plotted and presented in Figs. 8–10. It may be noted from Fig. 8 that the nature of the effectiveness curves predicted using the 2-D numerical model and that derived from the experiments, is similar. Effectiveness increases with the increase in the mass flow rate; it reaches a peak and then reduces. At the lower mass flow rates, larger ineffectiveness is observed due to AHC. Effect of AHC reduces with the increase in the mass flow rates and effectiveness reaches a peak at around 4 g/s. With further increase in the mass flow rate, effectiveness reduces due to reduction in the NTU. The computed mass flow rate for the peak effectiveness matches well with that derived from the experimental measurements (about 4 g/s). The experimentally derived effectiveness values are consistently higher than those computed using both the 2-D model as well as Aspen MUSE™ for different mass flow rates. At lower mass flow rates of around 2 g/s, experimentally derived effectiveness is found to be around 1.1% higher than that computed using the 2-D numerical model. As the flow rate increases, the difference between these two effectiveness gets reduced. At a mass flow rate of around 11 g/s, the derived effectiveness is about 0.5% higher than that computed from the 2-D model. Uncertainty in the experimentally derived effectiveness values is evaluated by sequentially perturbing the input process data and accumulating the individual uncertainty contributions [21]. For balanced flow heat exchanger, uncertainty in the experimentally derived effectiveness (around 0.3%) can be attributed mainly to the uncertainty in the measurement of temperature approach at high temperature end.

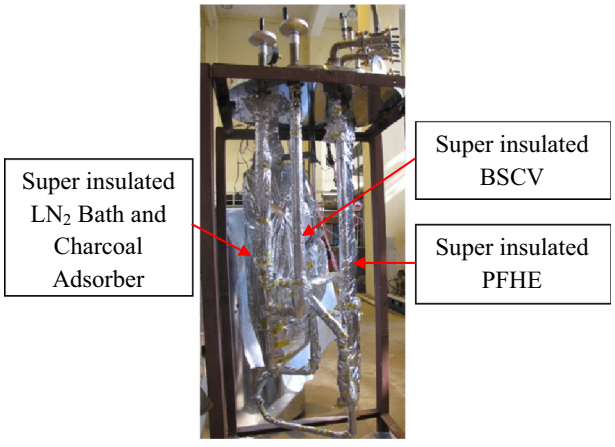

Fig. 6. The cold box piping with super insulation.

The effectiveness computed using Aspen MUSE™ [15] turns out to be higher at very low mass flow rates and lower at higher mass flow rates when compared to the experimentally derived effectiveness. As detailed in Fig. 8, the total metal cross-section area of the heat exchanger is 0.0028 m^2, but as per the output from Aspen MUSE™, effective cross-section area taken into account for AHC calculations is 0.0016 m^2 (AHC option: basic and fin). It is clear that for AHC computations, some proprietary factors are internally used in Aspen MUSE™ for estimating effective cross-section area vis a vis the actual one. It can be seen that although effectiveness computations with Aspen MUSE™ generally have a better match with the experimentally derived effectiveness as compared to the 2D numerical model, it under predicts the AHC effects at very low mass flow rates.

Comparison of effective overall heat transfer coefficient (UA), evaluated from experimentally measured and computed terminal temperatures based on Log Mean Temperature Difference (LMTD), for difference mass flow rates, is shown in Fig. 9 along with UA based on heat transfer area. Effective UA based on measured terminal temperatures is found to be consistently higher as compared to effective UA based on predicted terminal temperatures, a behavior similar to that exhibited by effectiveness curves as depicted in Fig. 8. The difference observed in UA values computed from the two methods may be attributed to AHC effects.

For mass flow rate of around 2 g/s, the HP and LP stream temperatures along the length of the heat exchanger, are plotted in Fig. 10. A sudden reduction in the HP stream temperature at the hot end and a similar sudden rise in the LP stream temperature at cold end is observed. This behavior is indicative of large AHC effects. The temperature approach along the major portion of the heat exchanger, as computed using the 2-D numerical model, is lower when compared to those obtained using Aspen MUSE™. This indicates that the numerical model over predicts the AHC effects as compared to Aspen MUSE™. Similarly, the difference between computed effectiveness using numerical model and that derived from experiments can only be justified through over estimation of AHC effects by the model.

From the experiments, results and the subsequent discussions presented in this article, it can be concluded that at higher mass flow rates, the 2-D numerical model [1] matches well with the experimental results and thus provides a fairly accurate description of the thermal hydraulic phenomenon inside PFHE channels. However, at lower mass flow rates, the numerical model over predicts the AHC effects, the reasons for which needs to be investigated and the model further improved to take care of the above mentioned discrepancy.

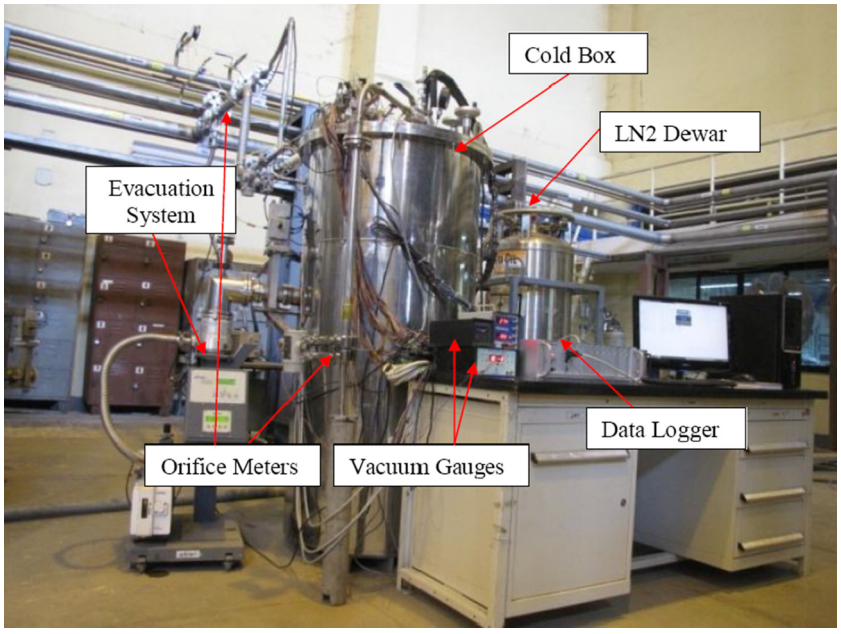

Fig. 7. The closed loop low temperature experimental test facility.

Table 2
Steady state process data at different mass flow rates for balanced flow case.

$\dot{m}_h$ (g/s) →	2.17			4.50			6.65			8.96			11.09		
Process Parameter↓	Exp.	Pred.		Exp.	Pred.		Exp.	Pred.		Exp.	Pred.		Exp.	Pred.	
		As per [1]	As per [15]		As per [1]	As per [15]		As per [1]	As per [15]		As per [1]	As per [15]		As per [1]	As per [15]
T_{hin} (K)	302.6			302.5			302.6			302.2			302.0		
T_{hexit} (K)	88.2	90.6	88.3	87.7	89.2	88.6	88.9	89.9	89.8	90.2	91.1	91.1	91.5	92.4	92.3
T_{cin} (K)	79.6			79.3			79.4			79.6			79.9		
T_{cexit} (K)	293.9	291.6	294.0	294.0	292.6	293.2	293.1	292.1	292.3	291.7	290.7	290.8	290.6	289.5	289.6
P_{hin} (bara)	1.37			1.57			1.84			2.18			2.58		
ΔP_h (mbar)	38	26	28	99	60	64	165	95	98	240	133	133	304	162	162
P_{cin} (bara)	1.29			1.32			1.36			1.42			1.48		
ΔP_c (mbar)	16	11	13	40	26	28	66	42	45	97	62	65	130	82	85
UA (W/K)	280	217	279	595	505	538	781	699	713	941	855	862	1090	970	976
ε	96.2	95.1	96.2	96.2	95.6	95.9	95.8	95.3	95.4	95.3	94.8	94.9	94.9	94.4	94.4

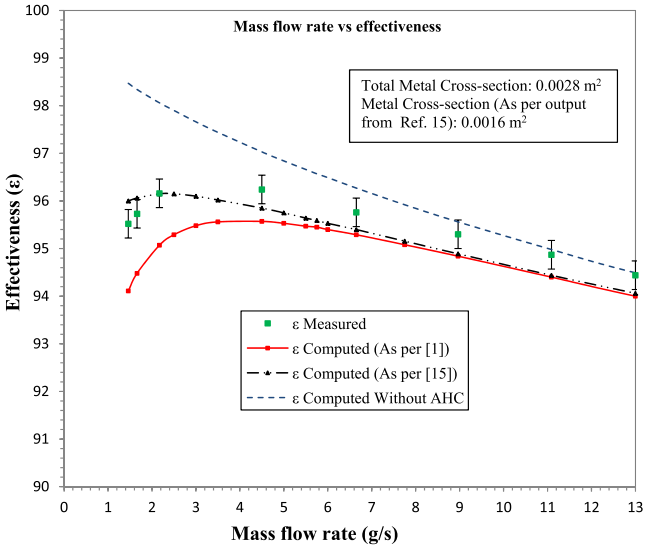

Fig. 8. Heat exchanger effectiveness for different mass flow rates.

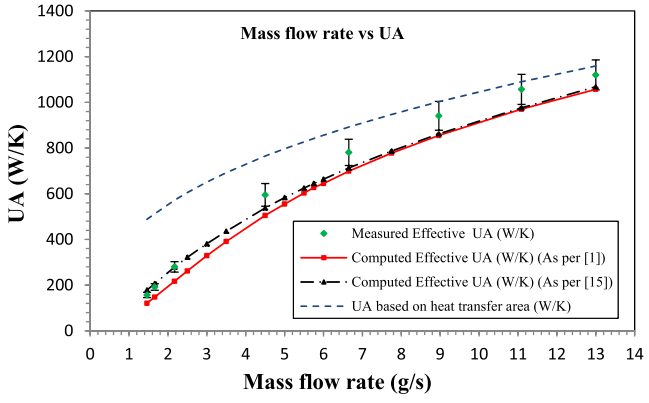

Fig. 9. Heat exchanger UA for different mass flow rates.

As shown in Table 2, for the HP stream, measured pressure drop is around 1.5 times the predicted core pressure drop at lower mass flow rates and it is around 1.9 times the predicted core pressure drop at higher mass flow rates. For the LP streams, measured pressure drop is around 1.5 times the predicted core pressure drop at

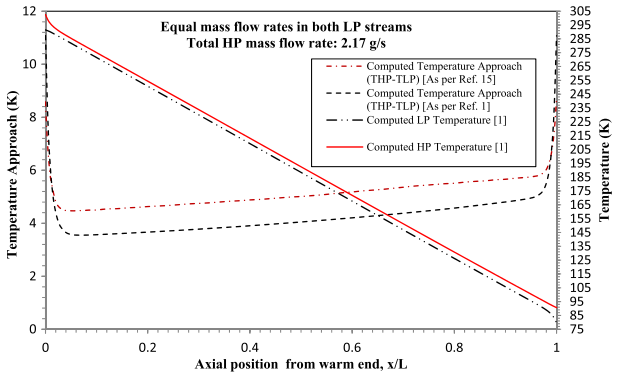

Fig. 10. Stream temperature profiles along the length of the PFHE.

lower mass flow rates and around 1.6 times the predicted core pressure drop at higher mass flow rates. It should be noted that the measured pressure drop is the total pressure drop including heat exchanger core, distributer, header and end connections, while the estimated pressure drop includes only the heat exchanger core pressure drop. In the used PFHE, there is only one layer (6.5 mm height) for each of the streams while the end connections are 1″ schedule 10 pipes. There may be substantial pressure drops in the header connecting 1″ diameter end connections to the layer having only 6.5 mm height. In larger multilayer heat exchangers, core pressure drops are higher compared to header pressure drops and hence the above observed discrepancy is not expected. The reasons for higher pressure drops need further investigations and CFD of the inlet headers/distributers can help in this regard.

Measured end plate temperatures along the length of the PFHE are compared for a total mass flow rate of 11 g/s with the predicted end plate temperatures as shown in Fig. 11. In general, measured end plate temperature profiles match well with those predicted from the numerical model. It is to be noted that for end plate temperature measurement, Pt-100 temperature sensors are pasted on the end plates using low temperature epoxy. It is observed that a few of the temperature sensors, especially at low temperature ends, have registered temperature values around 3–5 K higher than that predicted from the model. Sudden discontinuity in the measured temperature of the end plates is unrealistic and suggests the possibility of sensor mounting errors. Average difference

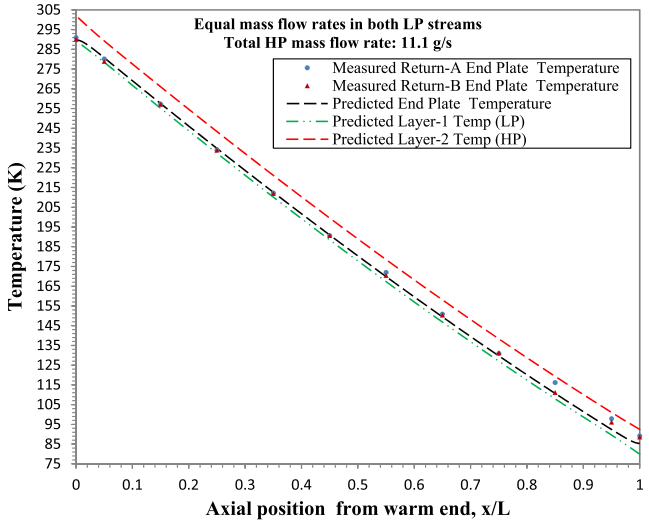

Fig. 11. End plate temperatures for the balanced flow two-stream case.

between the measured and the predicted end plate temperatures is 1 K while the absolute average difference is 1.6 K. If the inconsistent data registered by the improperly mounted sensors are neglected, average and absolute average difference between the measured and predicted end plate temperatures turns out to be 0 K and 0.7 K respectively.

5.2. Imbalanced flow two-stream case

For imbalanced flow experiments, two cases are selected for study. In Case-1, HP stream mass flow is higher than that in the LP stream. Whereas, in Case-2, the mass flow rate in the HP stream is lower.

For these experiments, steady state is first achieved with ≈6.8 g/s flow in both HP and LP streams (balanced flow case). Part of the flow from the exit of CA (Fig. 3) is then bypassed and fed directly to LP header after the LP return stream exit of the PFHE. Thus, the flow rate in the HP stream of the PFHE is higher than the flow through the LP stream. Similarly, for higher flow in the LP stream, additional gas is fed directly to the CA exit (Fig. 3) from the intermediate pressure buffer vessel of the closed loop compressor control system. Table 3 presents the steady state process data for both of the imbalanced cases. A comparison between the exit temperatures obtained experimentally with those predicted from the model [1] for the same inlet conditions, is also shown.

As depicted in Table 3, conservation of energy calculations between the streams throws up an error of 17 W for Case-1 and 21 W for Case-2. Measured effectiveness, for Case-1, is around 0.5% higher than the predicted effectiveness. Similarly, measured effectiveness, for Case-2, is around 0.3% higher than the predicted effectiveness. Uncertainty in the measured effectiveness is mainly due to uncertainty in the measurement of temperature approach at high temperature end and lower temperature end for Case-1 and Case-2 respectively. Total uncertainty in the measured effectiveness, is found to be around 0.3% for Case-1 and 0.8% and Case-2. Uncertainty in the predicted effectiveness for both cases, due to mass flow measurement is around 0.2%.

For Case-1, measured end plate temperatures along the length of the PFHE are compared, with the predictions as shown in Fig. 12. Measured end plate temperatures are found to be higher compared to the predicted ones and the average difference is 3.8 K. As discussed earlier, if the inconsistent data registered by the improperly mounted sensors are neglected, average difference between the measured and predicted end plate temperatures comes out to be 2.8 K. It is to be noted that in the case of imbalanced flow, temperature profile along the length of the PFHE strongly depends on the flow ratio between the hot and the cold streams. Therefore, difference between the measured and predicted end plate temperatures get affected by the flow measurement uncertainties.

5.3. Balanced flow three-stream case

For three-stream case, flow rate in both the LP streams should be different. Ratios of the mass flow rates of return-A and return-B are varied by using control valves BSCV-01 and BSCV-02. Table 4 presents the experimentally measured steady state process data for various flow ratios between the return A and the return B for a total mass flow rate of around 11.2 g/s. Measured process data are also compared with the predicted data for the same mass flow rates and inlet conditions which is shown in Table 4. It should be noted that the mass flow rate of the HP stream should be equal to the sum of the mass flow rates of the LP streams. Measured total flow rate of the LP streams is slightly different than the HP stream, maximum difference being 0.4% of the measured value. The above

Table 3
Steady state process data for the imbalanced flow.

Process Parameters↓	Case-1, higher flow in the HP stream			Case-2, lower flow in the HP stream		
	Exp.	Pred.	Diff.	Exp.	Pred.	Diff.
$\dot{m}_h$ (g/s)	6.77			6.31		
$\dot{m}_c$ (g/s)	6.28			6.75		
T_{hin} (K)	300.2			299.9		
T_{hexit} (K)	99.4	99.9	−0.6	97.9	98.5	−0.6
T_{cin} (K)	80.3			93.7		
T_{cexit} (K)	297.1	296.0	1.1	283.3	282.1	1.2
ε	98.6	98.1	0.5	98.0	97.7	0.3
Q_c-Q_h (W)	17			21		

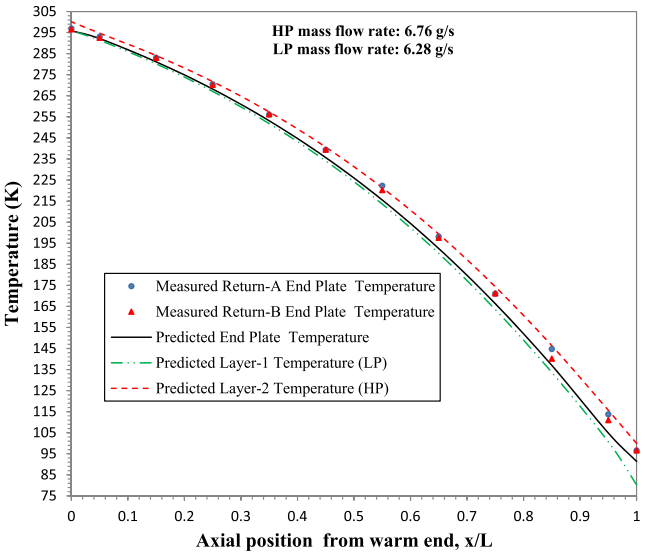

Fig. 12. End plate temperatures for the imbalanced flow two-stream case.

difference is due to uncertainty in the flow measurement. For performance prediction, the total LP mass flow rate is taken as equal to the HP mass flow rate and equal corrections are applied in both the LP streams. Inlet temperatures of both the LP streams should be equal as the same flow after the exit of CA (Fig. 3) is diverted to both LP streams. Any difference in the inlet temperatures of LP streams is due to temperature measurement uncertainty. For performance prediction, inlet temperatures of both the LP streams are taken as the inlet temperature of return B stream. In table 4, the effectiveness (ε_A) is defined as the effectiveness between return A and HP stream based on return-A stream. Similar definition is used for the effectiveness ε_B. The effectiveness (ε_{HP}) is defined as the effectiveness based on HP stream (LP stream temperature is taken as return B inlet temperature). Used expression for ε_A is given below:

$$\varepsilon_A = \frac{h_{exit,A} - h_{in,A}}{h^*_{exit,A} - h_{in,A}}$$

where h is enthalpy, $h^*_{exit,A}$ is enthalpy of return A LP stream at pressure $P_{exit,A}$ and temperature $T_{in,HP}$.

It is seen that for different flow ratios, measured performance matches well with the predicted one. The maximum difference between the predicted ε_{HP} and computed ε_{HP} based on measured temperatures is 0.3%. ε_{HP} is maximum when there is equal flow in both the return LP streams. In this case, PFHE is well balanced and half of the HP mass flow participates with the return A stream and half with the return B stream. As expected and shown in Table 4, overall performance of the PFHE (ε_{HP}) reduces with increase in the flow ratio ($\dot{m}_{returnB}/\dot{m}_{returnA}$). Mass flow participation in the heat transfer of the HP stream with the two return LP streams, in this case, is not proportional to the mass flow rates of the LP streams. As shown in Table 4, with increase in the flow ratio, measured ε_{HP} reduces from 94.5% to 93.5%. This degradation is similar to what happens when there is flow mal-distribution in a PFHE, with different flow rates in the different layers of a given fluid stream.

Measured end plate temperatures along the length of the PFHE are compared for a particular flow ratio with the predicted end plate temperatures in Fig. 13. In general, measured end plate temperature profiles match well with the predicted end temperature profiles from the model. Since the flow rates in both of the return streams are different, there exists a difference in the temperatures of the two end plates. Average difference between the measured and the predicted end plate temperatures is 1.1 K while the absolute average difference is 2.0 K. As discussed earlier, if the inconsistent data registered by the improperly mounted sensors are neglected, average and absolute average difference between the measured and predicted end plate temperatures turns out to be

Table 4
Steady state process data for different flow ratio between LP streams.

$\dot{m}_h$ (g/s) →	11.39			11.24			11.25		
Process Parameters↓	Exp.	Pred.	Diff.	Exp.	Pred.	Diff.	Exp.	Pred.	Diff.
$\dot{m}_{ReturnA}$ (g/s)	5.64	5.66		3.68	3.67		2.18	2.16	
$\dot{m}_{ReturnB}$ (g/s)	5.70	5.73		7.57	7.56		9.10	9.08	
Mass Flow Balance Error (g/s)	0.05			−0.01	0.00		−0.03		
T_{hin} (K)	302.1	302.1		302.0	302.0		301.7	301.7	
T_{hexit} (K)	92.0	92.5	−0.6	92.5	93.0	−0.5	94.3	94.3	−0.1
$T_{returnAin}$ (K)	80.3	79.8		80.4	79.8		80.8	79.9	
$T_{returnAexit}$ (K)	289.9	289.4	0.4	291.2	291.3	−0.1	291.5	292.6	−1.1
$T_{returnBin}$ (K)	79.8	79.8		79.8	79.8		79.9	79.9	
$T_{returnBexit}$ (K)	290.4	289.4	1.0	288.5	287.6	0.9	286.7	286.0	0.7
ε_A	94.5	94.3	0.2	95.1	95.2	−0.1	95.4	95.9	−0.5
ε_B	94.7	94.3	0.4	93.9	93.5	0.4	93.2	92.9	0.3
ε_{HP}	94.5	94.3	0.3	94.3	94.0	0.2	93.5	93.5	0.0

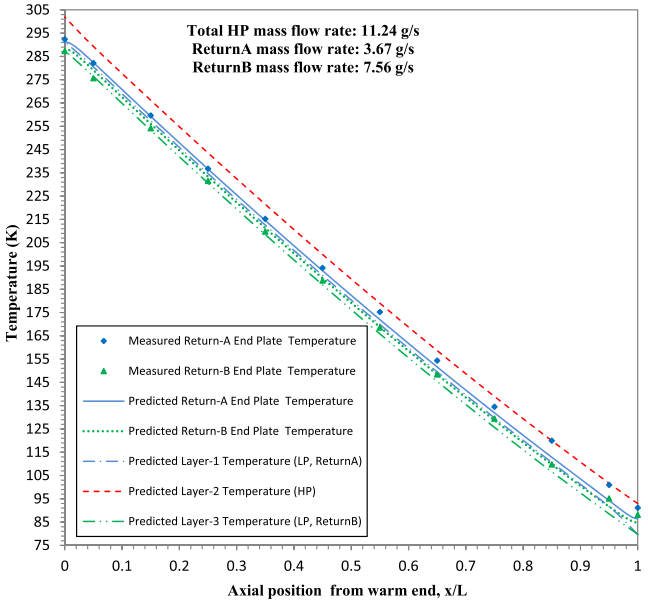

Fig. 13. End plate temperatures for the three-stream case.

−0.2 K and 1.0 K respectively. It is clearly seen in Fig. 13, is the presence of substantial temperature difference between two end plates and common wall temperature idealization [3] will be erroneous in such cases.

6. Conclusion

Exhaustive experiments at LN_2 temperatures are conducted, with a specially developed three-layer vacuum brazed aluminium PFHE, using a low temperature closed loop experimental test facility. Experimental studies included a two-stream balanced flow case with different mass flow rates, two-stream imbalanced flow case and three-stream case with different flow ratios between the two LP return streams. Experimental results are compared with those predicted using an earlier reported 2-D model for MSPFHE [1]. A reasonable match is found between the experimentally measured fluid exit temperatures and end plate temperatures along the length of the PFHE with the temperatures obtained from the model predictions. Hence, it can be concluded that the earlier reported 2-D model for MSPFHE stands validated now even at cryogenic temperatures, and the same can be conveniently used for PFHE design and analysis of different capacities and operating temperature ranges. At low mass flow rates, AHC is over predicted by the numerical model [1], the reasons should be investigated and the model can be further improved to take care of the above mentioned discrepancy. Similarly, reasons of higher pressure drops in the experimental results needs further investigations including pressure drop estimates in the headers/distributors.

Acknowledgements

The authors gratefully acknowledge the cooperation and help of colleagues from Cryo-Technology Division BARC for their help during fabrication of the test facility and experimental performance evaluation of heat exchanger.

References

[1] Goyal M, Chakravarty A, Atrey MD. Two dimensional model for multistream plate fin heat exchangers. Cryogenics 2014;61:70–8.
[2] Pacio JC, Dorao CA. A review on heat exchanger thermal hydraulic models for cryogenic applications. Cryogenics 2011;51(7):366–79.
[3] Das PK, Ghosh I. Thermal design of multistream plate fin heat exchanger – a state of the art review. Heat Transfer Eng 2012;33(4–5):284–300.
[4] Hu S, Herold KE. Prandtl number effect on offset fin heat exchanger performance: experimental results. Int J Heat Mass Transfer 1995;38(6):1053–61.
[5] Dong J, Chen J, Chen Z, Zhou Y. Air side thermal hydraulic performance of offset strip fin aluminum heat exchangers. Appl Therm Eng 2007;27:306–13.
[6] Peng H, Ling X. Numerical modeling and experimental investigation of flow and heat transfer over serrated fins at low Reynolds number. Exp Thermal Fluid Sci 2008;32:1039–48.
[7] Peng H, Ling X. Analysis of heat transfer and flow characteristics over serrated fins with different flow directions. Energy Convers Manage 2011;52:826–35.
[8] Du J, Qian Z, Dai Z. Experimental study and numerical simulation of flow and heat transfer performance on an offset plate fin heat exchanger. Heat Mass Transfer 2015. http://dx.doi.org/10.1007/s00231-015-1695-z.
[9] Wen J, Li Y, Zhou A, Zhang K. An experimental and numerical investigation of flow patterns in the entrance of plate fin heat exchanger. Int J Heat Mass Transfer 2006;49:1667–78.
[10] Wen J, Li Y, Zhou A, Zhang K, Wang J. PIV experimental investigation of entrance configuration on flow maldistribution in plate fin heat exchanger. Cryogenics 2006;46:37–48.
[11] Wen J, Li Y, Wang S, Zhou A. Experimental investigation of header configuration improvement in plate fin heat exchanger. Appl Therm Sci 2007;27:1761–70.
[12] Ismail LS, Ranganayakulu C, Shah RK. Numerical study of flow patterns of compact plate-fin heat exchangers and generation of design data for offset and wavy fins. Int J Heat Mass Transfer 2009;52:3972–83.
[13] Doohan RS, Kush PK, Maheshwari G. Exergy based optimization and experimental evaluation of plate fin heat exchanger. Appl Therm Eng 2016;102:80–90.
[14] Wang Z, Li Y, Zhao M. Experimental investigation on the thermal performance of multistream plate fin heat exchanger based on genetic algorithm layer pattern design. Int J Heat Mass Transfer 2015;82:510–20.
[15] AspenONE. Aspen MUSE™, version 2004.1. AspenTech India Pvt.
[16] Users guide to GASPAK®, version 3.35/3.45. Horizon Technologies; October 2007. <http://www.htess.com>.
[17] Users guide to HEPAK®, version 3.40/3.41. Horizon Technologies; March 2005. <http://www.htess.com>.
[18] NIST Cryogenics Technologies Group, "Material Properties". <http://cryogenics.nist.gov/MPropsMAY/materia/properties.html>.
[19] Manglik RM, Bergles AE. Heat transfer and pressure drop correlations for the rectangular offset strip fin compact heat exchanger. Exp Thermal Fluid Sci 1995;10(2):171–80.
[20] The American society of mechanical engineers rules for construction of pressure vessels 2003 ASME Sec VIII Div I.
[21] Moffat RJ. Describing the uncertainties in experimental results. Exp Thermal Fluid Sci 1998;1:3–17.